ACS APPLIED MATERIALS & INTERFACES

Research Article

www.acsami.org

Spatial Atmospheric Atomic Layer Deposition of $Al_xZn_{1-x}O$

A. Illiberi,*[,†] R. Scherpenborg,[†] Y. Wu,[‡] F. Roozeboom,[†,‡] and P. Poodt[†]

[†]Holst Centre/TNO Thin Film Technology, P.O. Box 6235, 5600 HE Eindhoven, The Netherlands

[‡]Department of Applied Physics, Eindhoven University of Technology, P.O. Box 513, 5600 MB Eindhoven, The Netherlands

ABSTRACT: The possibility of growing multicomponent oxides by spatial atmospheric atomic layer deposition has been investigated. To this end, $Al_xZn_{1-x}O$ films have been deposited using diethyl zinc (DEZ), trimethyl aluminum (TMA), and water as Zn, Al, and O precursors, respectively. When the metal precursors (i.e., TMA and DEZ) are coinjected in the deposition region, the Al/(Al + Zn) ratio can be accurately controlled by either varying the TMA flow to the reactor or the exposure time of the substrate to the precursors. A high doping efficiency level (up to 70%) is achieved in Al-doped ZnO, resulting in films with a high carrier density (5×10^{20} cm^{-3}), low resistivity (2×10^{-3} Ω cm), and good optical transparency (>85%) in the visible range. The morphology of the films changes from polycrystalline, in conductive i-ZnO and Al-doped ZnO, to amorphous, in highly resistive Al-rich films. The unique combination of the fine tuning of the composition, morphology, and electrical properties of the films with high deposition rates (>0.2 nm/s) paves the way for spatial ALD as an emerging disruptive technique for the growth of multicomponent oxides over large areas.

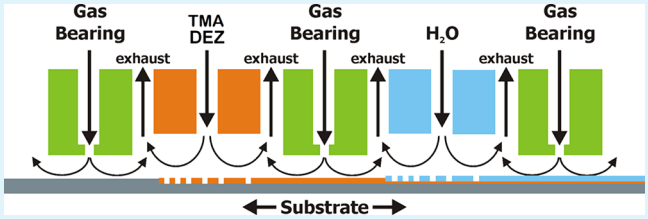

KEYWORDS: *atomic layer deposition, atmospheric pressure, transparent conductive oxides, multicomponent oxide, zinc oxide, aluminum oxide*

INTRODUCTION

Multicomponent oxides have found an increasing number of industrial applications because their physical properties, including refractive index, surface roughness, hardness, and conductivity, can be controlled over a wide range by varying the film stoichiometry.[1,2] Several methods for the deposition of multicomponent oxides have been proposed, including sputtering, chemical vapor deposition, sol−gel growth, and atomic layer deposition (ALD).[3−5] Conventionally, the ALD technique is characterized by the time-sequenced introduction of the precursors in the deposition zone, where selective and self-limiting half reactions occur on the substrate, thus allowing digital control of the film thickness. The industrial need for uniform, pinhole free, and highly conformal thin films on large-area and flexible substrates has driven the recent development of multicomponent oxides by ALD.

ALD of multicomponent oxides is typically performed by alternating the self-limiting growth of binary oxide layers.[5−8] Although this allows for the precise control of the average film stoichiometry, the concentrations of the different metal elements and the physical properties of the films are strongly inhomogeneous along the growth direction.[9,10] In the case of doped metal oxides (e.g., Al-doped ZnO), various approaches have been proposed to control the spatial distribution of the doping elements (e.g., Al), such as employing precursors with a low growth rate per cycle, a subsaturating dopant precursor exposure, or a surface functionalization step.[11−13]

Although ALD combines superior conformality with excellent film uniformity, it cannot meet the industrial requirements for high-throughput deposition rates corresponding to several hundreds of nanometers per minute. This drawback has been overcome by the development of spatial ALD, where the dosage of the precursors occurs in different space-divided zones of the reactor, and a moving substrate is sequentially exposed to each of these zones. By spatially dividing the zones by a nitrogen gas curtain, a purge step is no longer needed, and deposition rates as high as nanometers per second have been achieved.[14] Atmospheric pressure spatial ALD is emerging as an industrially scalable technique for the deposition of thin-film electrodes (e.g., ZnO) and encapsulation (e.g., by Al_2O_3 thin films) of solar and electronic devices.[15,16]

In recent years, Al-doped ZnO (ZnO:Al) has received increasing interest because it combines the common properties of transparent conductive oxides (i.e., low resistivity and excellent transparency) with low cost, low toxicity, easy fabrication process and patterning.[1] Low values of resistivity (∼ 10^{-4} Ω cm), high carrier mobility (∼ 50 $cm^2/(V\ s)$), and high transparency in the visible range (> 90 %) have been achieved in ZnO:Al grown at low temperatures (< 200 °C).[17] Therefore, ZnO:Al is a valid and cheaper alternative to both the commonly used indium tin oxide or the emerging graphene-based electronics for applications in flexible devices.[18]

Although ALD ZnO:Al is conducting and polycrystalline, Al_2O_3 is insulating and amorphous so that the physical properties of $Al_xZn_{1-x}O$ films may span a broad range depending on their stoichiometry. For this reason, $Al_xZn_{1-x}O$

Received: September 23, 2013
Accepted: December 2, 2013
Published: December 2, 2013

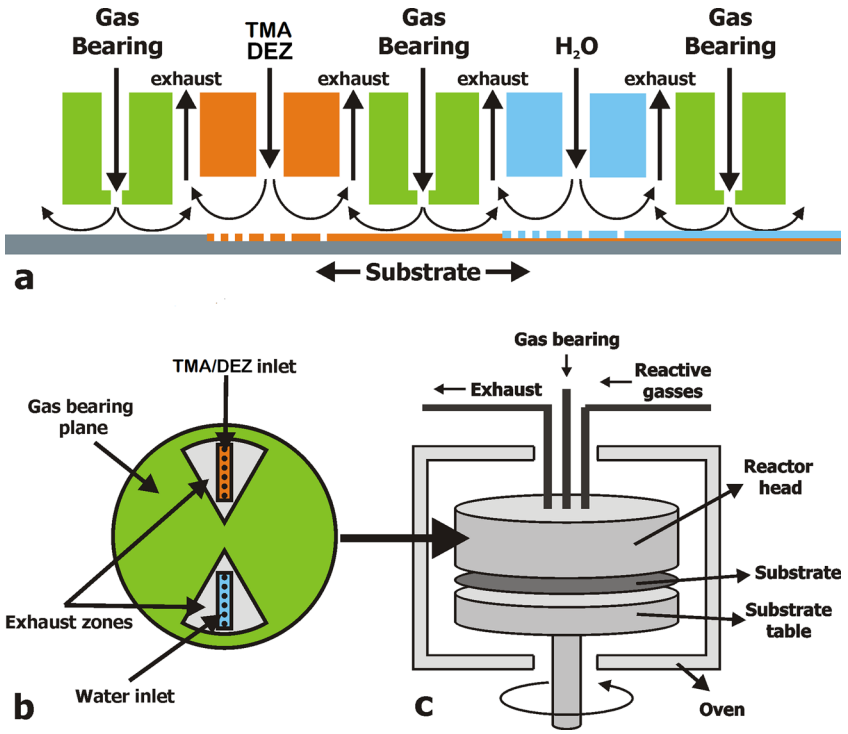

Figure 1. (a) Schematic drawing of the spatial ALD reactor (from ref 14). The TMA/DEZ and water half-reaction zones are separated by gas bearings. By moving the substrate underneath the reactor, the two half reactions take place subsequently to form an $Al_xZn_{1-x}O$ monolayer. (b) Schematic drawing of the bottom side of the spatial ALD reactor head, where the TMA/DEZ and water half-reaction zones are integrated into inlets surrounded by exhaust zones and gas-bearing planes. The colors correspond to those in panel a. (c) Schematic drawing of the reactor.

thin films have been selected to investigate the growth of multicomponent oxides by spatial ALD.

EXPERIMENTAL SECTION

A schematic of the atmospheric spatial ALD reactor used for the deposition is shown in Figure 1. Two different inlets are installed in the circular gas-injection head, one for the metal precursors and another for the oxygen precursor. The vaporized precursors are injected continuously into the deposition zone via the inlets. The substrate is placed on a circular table that rotates underneath the reactor head at a distance of typically 20−100 μm. During each rotation, the substrate is exposed sequentially to each precursor. Between and around the reactant inlets, shields of inert gas (10 slm of N_2) separate the precursor flows and seal off the reaction zones, thus making the reactor completely independent of the environment, enabling operation under atmospheric pressure conditions. The entire reactor is installed in a conventional oven that can be heated to 400 °C.

For the conditions reported in this article, diethyl zinc [$Zn(C_2H_5)_2$, (DEZ)], trimethyl aluminum [$Al_2(CH_3)_6$, (TMA)], and water (H_2O) vapor were used as zinc, aluminum, and oxygen precursors, respectively. Metal precursors and deionized water were evaporated from bubblers by using argon as a carrier gas and transported to the reactor head through heated lines to prevent condensation. The DEZ and TMA bubblers were heated in thermostatic water baths at 32 °C to control the vapor pressure of the precursors, whereas the H_2O bubbler was kept at 50 °C.

The argon flow through the H_2O and DEZ bubbler was set at 1000 and 70 sccm, respectively, whereas the argon flow through the TMA bubbler was varied (0, 2, 3, 5, 10, 15, 18, and 30 sccm). The flows from the DEZ and TMA bubblers were mixed and coinjected in the deposition zone through the same inlet after being diluted by argon. The dilution flow was adjusted to 930, 928, 927, 925, 920, 915, 912, 900 sccm for each value of argon flow through the TMA bubbler so that the total flow in the inlet was kept constant at 1000 sccm. A rotation frequency of 1.7 Hz, a total number of 1500 ALD cycles, and a substrate temperature of 200 °C were set for the depositions reported here.

A ∼4 cm wide ring-shaped track of $Al_xZn_{1-x}O$ was deposited on 15 × 15 cm^2 glass substrates (Schott AF 32), corresponding to the width and position of the deposition inlets (Figure 1b). The glass substrates were cleaned by ethanol, rinsed by water, and subsequently blow-dried with nitrogen. The electrical properties and thickness of the films were determined using a Phystech RH 2010 Hall-effect measurement system, a Jandel universal four-point probe, and a Veeco Dektek 8 advanced development profiler, respectively. Film optical properties were measured in the near-ultraviolet, visible, and near-infrared ranges by a UV-3600 Shimadzu spectrophotometer. A Philips X-pert SR5068 powder diffractometer equipped with a Cu Kα source was used to determine the crystallographic structure of the films. The zinc and aluminum contents in the films were measured both in a FEI Quanta 600 FEG SEM system equipped with an energy-dispersive X-ray (EDX) diagnostic and in a Quantera system from ULVAC-PHI (Q2) equipped with X-ray photoelectron spectroscopy (XPS). For the XPS analysis, a spectrophotometer with monochromatic Al Kα X-ray radiation ($h\nu$ = 1486.6 eV, 25 Watt, 100 μm spot size) was used. Photoelectrons were collected at a take-off angle of 51°, as measured from the surface normal. Concentration-depth profiles of Zn, Al, O, and C were measured by alternately measuring and sputtering with 4.0 kV Ar^+ ions over an area of 3 × 3 mm^2.

RESULTS AND DISCUSSION

Spatial ALD of Al_2O_3 and intrinsic ZnO (i-ZnO) was recently investigated using TMA or DEZ as metal precursors, respectively, and H_2O.[15,19] For the spatial ALD of $Al_xZn_{1-x}O$, the DEZ molar flow to the reactor was kept constant at 95 μmol/min, whereas the coinjected TMA flow ranges from 0 to 57 μmol/min and the exposure time is varied in the range from 36 to 156 ms. When TMA is not injected in the deposition zone, i-ZnO films are grown at a rate of ∼0.20 nm/cycle,

dx.doi.org/10.1021/am404137e | ACS Appl. Mater. Interfaces 2013, 5, 13124−13128

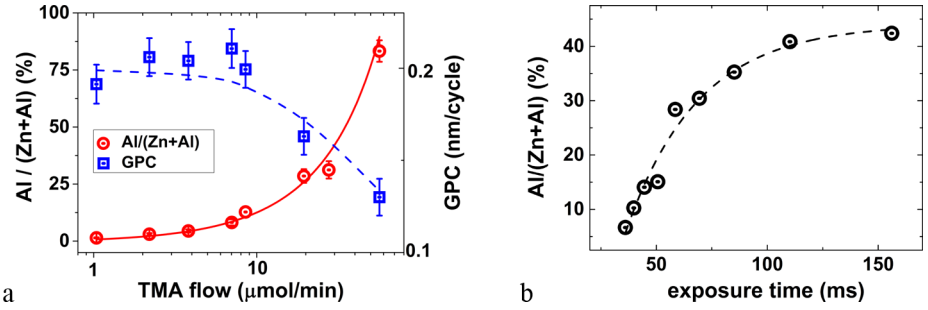

Figure 2. (a) Al/(Al + Zn) ratio measured by EDX and growth per cycle versus TMA flow to the reactor for a constant exposure time of 60 ms and DEZ molar flow of 95 μmol/min. (b) Al/(Al + Zn) ratio versus exposure time of the substrate to the metal precursors. TMA and DEZ flows were kept constant at 20 and 95 μmol/min, respectively.

similar to what has been reported for the self-saturated growth of i-ZnO by conventional ALD.

As shown in Figure 2a, the Al/(Zn + Al) ratio varies from 0 to 83% with the TMA flow increasing from 0 to 57 μmol/min at a constant exposure time of 60 ms. A sharp increase in the Al/(Zn + Al) ratio from 6 to 42% was found when increasing the exposure time from 36 to 156 ms at a constant TMA flow of 20 μmol/min, as shown in Figure 2b. Because DEZ and TMA vapors are coinjected continuously in the same deposition region, the reaction steps between surface hydroxyl groups and the two metal precursors can occur simultaneously, producing both $Zn(C_2H_5)$ and $Al(CH_3)_2$ surface species. Although the competitive adsorption of TMA and DEZ at surface hydroxyl groups results in a time-independent Al/(Zn + Al) ratio, we observed an increase of the Al content with exposure time (Figure 2b).[21] This suggests that besides a competitive adsorption process, TMA molecules can also etch the chemisorbed DEZ, possibly via a CH_3 ligand-exchange reaction.

Etching of Zn by TMA exposure has been observed previously during the deposition of Al_2O_3/ZnO nanolaminates by conventional ALD.[5,6] The Zn content in the Al_2O_3/ZnO nanolaminates was reported to be significantly below the expected values, and a loss in deposited mass was detected by quartz crystal microbalance during each TMA pulse that follows a DEZ pulse.[5] The experimental results can be understood by considering that O−Zn−(C_2H_5) surface species are replaced by Al-methyls, resulting in the formation of both volatile Zn-alkyls, which can react again with surface hydroxyle groups, and surface O−Al-alkyls, which are stable under DEZ exposure. Gas-phase products of this reaction were measured by in situ quadrupole mass spectroscopy, and the primary volatile desorbing species were identified as $Zn(CH_3)_2$.[20] It has been proposed that etching of Zn by TMA occurs because of the larger formation enthalpy of Al_2O_3 (−845 kJ/mol Al atoms) compared to ZnO (−353 kJ/mol Zn atoms).[20] Under these conditions, the $-Zn(C_2H_5)$ surface species act partially as a sacrificial layer, which facilitates controlling the incorporation of Al atoms in the film.

The growth per cycle (GPC) of multicomponent oxides should ideally correspond to a linear combination of the GPC of each binary oxide comprising the film, which for $Al_xZn_{1-x}O$ is

$$GPC = N_{cycles}[(Zn\%)GPC_{ZnO} + (100 - Zn\%)/100GPC_{Al_2O_3}] \quad (1)$$

where N_{cycles} is the number of cycles, Zn% is the Zn content, and GPC_{ZnO} = 0.20 nm/cycles and $GPC_{Al_2O_3}$ = 0.12 nm/cycles, which is the growth per cycle of i-ZnO and Al_2O_3 films, respectively. When $Al_xZn_{1-x}O$ films are deposited by alternating the individual subcycles of self-limiting growth of Al_2O_3 and ZnO layers, the net GPC deviates strongly from eq 1. This is due to a nucleation period of each binary oxide on the different metal-oxide substrate, thus resulting in a poor control of the film thickness.[5] The GPC of spatial ALD $Al_xZn_{1-x}O$ versus TMA flow is shown in Figure 2a. The experimental data follow the GPC expected from eq 1, indicating that the coinjection of the metal precursors allows for optimum control of the film thickness, as is also shown in ref 22. A GPC varying from 0.12 to 0.20 nm/cycle at a rotation frequency of 1.7 Hz results in a growth rate of 0.2 to 0.33 nm/s, respectively, which is comparable with the growth rates of other industrial-deposition techniques, such as sputtering.[1]

XRD spectra of $Al_xZn_{1-x}O$ films are shown in Figure 3. As reported in a previous study, spatial ALD i-ZnO films have a

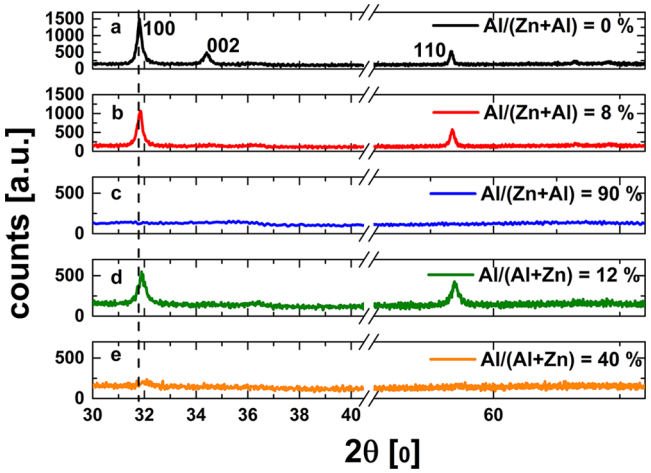

Figure 3. XRD spectra of $Al_xZn_{1-x}O$ films with varying TMA exposure: (a) 0, (b) 7, and (c) 57 μmol/min at 60 ms constant exposure time; (d) 60 and (e) 125 ms at a constant TMA flow rate of 20 μmol/min.

polycrystalline structure with a dominant (100) orientation, although other orientations are clearly visible.[15] Figure 3b,d shows that the incorporation of Al atoms into the ZnO lattice induces a degradation of the crystalline structure, resulting in a lower intensity of the crystalline peaks and a systematic shift of the peaks to higher angles (2θ = 31.8° for i-ZnO and 2θ = 31.9°

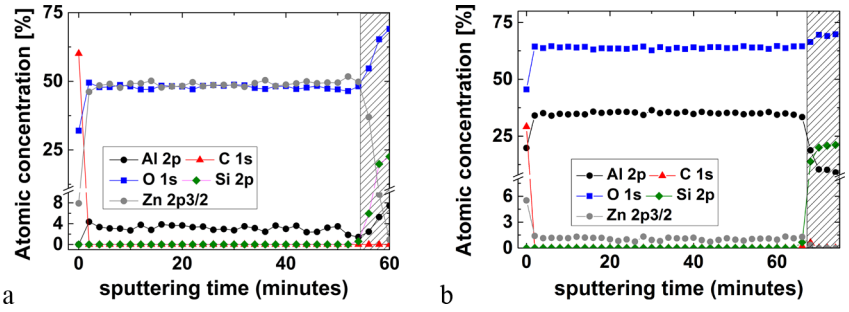

Figure 4. XPS concentration-depth profiles of Al, Zn, O, and C elements in (a) Zn-rich and (b) Al-rich $Al_xZn_{1-x}O$ films for a TMA flow of 7 and 57 μmol/min and exposure times of 60 and 80 ms, respectively. The segmented areas refer to the glass substrate.

for Al/(Al + Zn) = 12%). This shift is attributed to the Al substitution on a Zn site, leading to a decrease of the lattice constant because of the smaller ionic radius of Al^{3+} (0.53 Å) with respect to Zn^{2+} (0.72 Å).[22] With further increasing of the Al content via either a higher TMA flow (Figure 3c) or a longer exposure time (Figure 3e), the films obtain an amorphous structure similar to Al_2O_3.

The bulk composition of Zn-rich and Al-rich $Al_xZn_{1-x}O$ films was determined by X-ray photoelectron spectroscopy. The XPS depth profiles of $Al_xZn_{1-x}O$ with Al/(Al + Zn) = 7 and 96% are shown in Figure 4. For the settings used in the XPS analysis, the atomic distribution of the different elements (Al, Zn, O, and C) can be measured along the growth direction with a resolution of ~7 nm.[10] In both films, the carbon concentration is below the detection limit after sputter removal of the top layers that were exposed to atmosphere prior to analysis. A nearly constant concentration-depth profile for Al and Zn elements was measured in both $Al_xZn_{1-x}O$ films, within the resolution limit of the XPS analysis.

In the remaining part of this work, we have investigated the electrical and optical properties of the $Al_xZn_{1-x}O$ films. The resistivity (ρ) is defined as $\rho = Rd$, where the sheet resistance (R) is determined from four-point probe measurements, and the thickness (d) is obtained using a step profiler. As shown in Figure 5, the resistivity decreases sharply with increasing Al content, passing from a value of 0.1 Ω cm for i-ZnO to a minimum value of 2×10^{-3} Ω cm for Al/(Al + Zn) = 8%.

The improvement in the electrical properties is mainly due to a sharp increase in carrier density, which passes from 7×10^{18} cm^{-3} in i-ZnO to 5×10^{20} cm^{-3} at Al/(Al + Zn) = 8%, giving a value of carrier mobility of about 5 $cm^2/(V\ s)$. Although the optimum value of Al/(Al + Zn) to achieve the lowest resistivity agrees with previous results reported in the literature, the corresponding carrier density is much higher than for Al-doped ZnO by conventional ALD (i.e., 2×10^{20} cm^{-3}).[23] This suggests that a higher doping efficiency is achieved in spatial ALD $Al_xZn_{1-x}O$. Assuming that one Al atom donates at most one free-electron, the doping efficiency (ζ) can be calculated as

$$\zeta = \frac{N_e - N_{e0}}{\mathrm{Al}\% \frac{\sigma}{2M_{mol}} N_A} \quad (2)$$

where N_e is the carrier density of Al:ZnO, N_{e0} is carrier density in i-ZnO evaluated by Hall measurements, Al% is the aluminum content as determined by EDX, σ is the ZnO density, which is taken to be the bulk density (5.606 g/cm^3), M_{mol} is the molar mass of ZnO (81.4 g/mol), and N_A is Avogadro's constant. Conventional ALD of Al-doped ZnO is typically performed by inserting Al_2O_3 growth cycles in the growth of i-ZnO.[5−8] This implies that Al donors are localized in planes perpendicular to the growth direction, resulting in a low doping efficiency (<15%) because of the formation of Al−O−Al clusters or to the Coulomb repulsion force between adjacent charged Al atoms, which suppress the donation of electrons.[6,24] On the contrary, a maximum doping efficiency of about 70% was achieved in spatial ALD $Al_xZn_{1-x}O$ with Al/(Al + Zn) = 1.4%. Similar values of doping efficiency are reported for Al-doped ZnO grown by other industrially scalable deposition techniques, such as sputtering, or by conventional ALD, when controlling the Al distribution along the growth direction by either coinjecting the metal precursors and using O_3 as oxidizer or by functionalizing the film surface.[6,12,22,25]

The transmittance of $Al_xZn_{1-x}O$ films was measured in the range from 280 to 2500 nm, and the results are shown in Figure 6. All films are highly transparent (>85%) in the visible range, whereas the transparency decreases in the near-infrared range

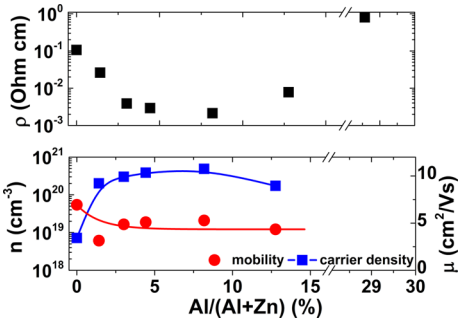

Figure 5. Resistivity (top) and carrier density and mobility (bottom) versus Al content with varying TMA flow from 0 to 20 μmol/min at constant exposure time of 60 ms. Hall measurements cannot be performed in highly resistive films (R > 1000 Ω/sq).

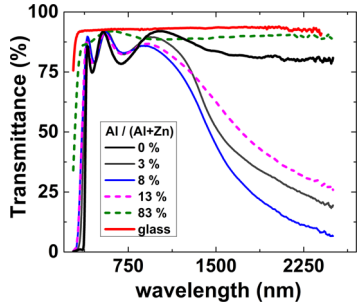

Figure 6. Transparency of $Al_xZn_{1-x}O$ films and glass substrate with varying Al content using the same deposition conditions described in the caption of Figure 5

as Al/(Al + Zn) increases from 0 to 8% because of free carrier absorption.

As shown in Figure 6, a further increase in Al content from 8 to 13 and to 83% results in a decreased carrier density and in a much higher film resistivity (up to 0.8 Ω cm) because of the possible formation of an insulating $ZnAl_2O_4$ spinel or $(ZnO)_3(Al_2O_3)$ phase.[7,26] The decrease in carrier density and the formation of Al_xO_y phases induce a higher transparency in the near-infrared range and a blue shift of the optical band gap, respectively, as shown in Figure 6.[27]

CONCLUSIONS

$Al_xZn_{1-x}O$ was grown by atmospheric pressure spatial ALD. We have shown that by coinjecting the metal precursors (DEZ and TMA) in the same deposition region, the stoichiometry of the films can be accurately controlled. $Al_xZn_{1-x}O$ films with high Al content are amorphous insulators, whereas they become polycrystalline transparent conductors at high Zn content. We expect that the possibility of fine tuning the composition, morphology, and electrical properties of the $Al_xZn_{1-x}O$ films combined with high deposition rates (> 0.2 nm/s) over large areas makes spatial ALD a unique technique for the growth of these films as well as other multicomponent oxides.

AUTHOR INFORMATION

Corresponding Author

*E-mail: andrea.illiberi@tno.nl.

Notes

The authors declare no competing financial interest.

REFERENCES

(1) *Handbook of Transparent Conductors*; Ginley, D., Hosono, H., Paine, D. C., Eds.; Springer: New York, 2011; p 534.
(2) Elam, J. W.; Sechrist, Z. A.; George, S. M. *Thin Solid Films* **2002**, *414*, 43.
(3) Lim, J. H.; Shim, J. H.; Choi, J. H.; Joo, J.; Park, K.; Jeon, H.; Moon, M. R.; Jung, D.; Kim, H.; Lee, H. J. *Appl. Phys. Lett.* **2009**, *95*, 012108.
(4) Minami, T. *J. Vac. Sci. Technol., A* **1999**, *17*, 1765.
(5) Elam, J. W.; George, S. M. *Chem. Mater.* **2003**, *15*, 1020.
(6) Na, J. S.; Peng, Q.; Scarel, G.; Parson, G. N. *Chem. Mater.* **2009**, *21*, 5585.
(7) Banerjee, P.; Lee, W. J.; Bae, K. R.; Lee, S. B.; Rubloff, G. W. *J. Appl. Phys.* **2010**, *108*, 043504.
(8) Geng, Y.; Guo, L.; Xu, S. S.; Sun, Q. Q.; Ding, S. J.; Lu, H. L.; Zhang, D. W. *J. Phys. Chem. C.* **2011**, *115*, 12317.
(9) Na, J. S.; Scarel, G.; Parsons, G. N. *J. Phys. Chem. C.* **2010**, *114*, 383.
(10) Wu, Y.; Hermkens, P. M.; van de Loo, B. W. H.; Knoops, H. C. M.; Potts, S. E.; Verheijen, M. A.; Roozeboom, F.; Kessels, W. M. M. *J. Appl. Phys.* **2013**, *114*, 024308.
(11) Kim, J. Y.; Choi, Y. J.; Park, H. H.; Golledge, S.; Johnson, D. C. *J. Vac. Sci. Technol., A* **2010**, *28*, 1111.
(12) Yanguas-Gil, A.; Peterson, K. E.; Elam, J. *Chem. Mater.* **2011**, *23*, 4295.
(13) Van, T. T.; Chang, J. P. *Appl. Phys. Lett.* **2005**, *87*, 011907.
(14) Poodt, P.; Lankhorst, A.; Roozeboom, F.; Spee, K.; Maas, D.; Vermeer, A. *Adv. Mater.* **2010**, *22*, 3564.
(15) Illiberi, A.; Roozeboom, F.; Poodt, P. *ACS. Appl. Mater. Interfaces* **2012**, *4*, 268.
(16) Illiberi, A.; Scherpenborg, R.; Theelen, M.; Poodt, P.; Roozeboom, F. *J. Vac. Sci. Technol., A* **2013**, *31*, 061504.
(17) Tanaka, H.; Ihara, K.; Miyata, T.; Sato, H.; Minami, T. *J. Vac. Sci. Technol., A* **2004**, *22*, 1757.
(18) Feng, H.; Cheng, R.; Zhao, X.; Duan, X.; Li, J. *Nat. Commun.* **2012**, *4*, 1539.
(19) Poodt, P.; van Lieshout, J.; Illiberi, A.; Knaapen, R.; Roozeboom, F.; van Asten, A. *J. Vac. Sci. Technol., A* **2013**, *31*, 01A108.
(20) Elam, J. W.; Libera, J. A.; Pellin, M. J.; Stair, P. C. *Appl. Phys. Lett.* **2007**, *91*, 243105.
(21) Puurunen, R. L. *J. Appl. Phys.* **2005**, *97*, 121301.
(22) Yuan, H.; Luo, B.; Yu, D.; Cheng, A.; Campbell, S. A.; Gladfelter, W. L. *J. Vac. Sci. Technol., A* **2012**, *30*, 01A138.
(23) Lujala, V.; Skarp, J.; Tammenmaa, M.; Suntola, T. *Appl. Surf. Sci.* **1994**, *82*, 34.
(24) Lee, D. J.; Kim, H. M.; Kwon, J.Y.; Choi, H.; Kim, S. H.; Kim, K. B. *Adv. Funct. Mater.* **2011**, *21*, 448.
(25) Hu, J.; Gordon, R. G. *J. Appl. Phys.* **1992**, *71*, 880.
(26) Yoshioka, S.; Oba, F.; Huang, R.; Tanaka, I.; Mizoguchi, T.; Yamamoto, T. *J. Appl. Phys.* **2008**, *103*, 014309.
(27) Vinnichenko, M.; Gago, R.; Cornelius, S.; Shevchenko, N.; Rogozin, A.; Kolitsch, A.; Munnik, F.; Moller, W. *Appl. Phys. Lett.* **2010**, *96*, 141907.